Evaluation of the AMPS Boundary Layer Simulations on the Ross Ice Shelf, Antarctica, with Unmanned Aircraft Observations

JONATHAN D. WILLE AND DAVID H. BROMWICH

Polar Meteorology Group, Byrd Polar and Climate Research Center, The Ohio State University, Columbus, Ohio

JOHN J. CASSANO

Cooperative Institute for Research in Environmental Sciences, and Department of Atmospheric and Oceanic Sciences, University of Colorado Boulder, Boulder, Colorado

MELISSA A. NIGRO

Department of Atmospheric and Oceanic Sciences, University of Colorado Boulder, Boulder, Colorado

MARIAN E. MATELING

Antarctic Meteorological Research Center, Space Science and Engineering Center, and Department of Atmospheric and Oceanic Sciences, University of Wisconsin–Madison, Madison, Wisconsin

MATTHEW A. LAZZARA

Antarctic Meteorological Research Center, Space Science and Engineering Center, University of Wisconsin–Madison, and Department of Physical Sciences, School of Arts and Sciences, Madison Area Technical College, Madison, Wisconsin

(Manuscript received 12 October 2016, in final form 10 April 2017)

ABSTRACT

Accurately predicting moisture and stability in the Antarctic planetary boundary layer (PBL) is essential for low-cloud forecasts, especially when Antarctic forecasters often use relative humidity as a proxy for cloud cover. These forecasters typically rely on the Antarctic Mesoscale Prediction System (AMPS) Polar Weather Research and Forecasting (Polar WRF) Model for high-resolution forecasts. To complement the PBL observations from the 30-m Alexander Tall Tower! (ATT) on the Ross Ice Shelf as discussed in a recent paper by Wille and coworkers, a field campaign was conducted at the ATT site from 13 to 26 January 2014 using Small Unmanned Meteorological Observer (SUMO) aerial systems to collect PBL data. The 3-km-resolution AMPS forecast output is combined with the global European Centre for Medium-Range Weather Forecasts interim reanalysis (ERAI), SUMO flights, and ATT data to describe atmospheric conditions on the Ross Ice Shelf. The SUMO comparison showed that AMPS had an average 2–3 m s^{-1} high wind speed bias from the near surface to 600 m, which led to excessive mechanical mixing and reduced stability in the PBL. As discussed in previous Polar WRF studies, the Mellor–Yamada–Janjić PBL scheme is likely responsible for the high wind speed bias. The SUMO comparison also showed a near-surface 10–15-percentage-point dry relative humidity bias in AMPS that increased to a 25–30-percentage-point deficit from 200 to 400 m above the surface. A large dry bias at these critical heights for aircraft operations implies poor AMPS low-cloud forecasts. The ERAI showed that the katabatic flow from the Transantarctic Mountains is unrealistically dry in AMPS.

1. Introduction

Properly modeling the planetary boundary layer (PBL) over the Antarctic ice sheets is essential for maintaining a high degree of efficiency and safety for the U.S. Antarctic Program (USAP)'s flight operations. The

Contribution 1546 of Byrd Polar and Climate Research Center.

Corresponding author: David H. Bromwich, bromwich.1@osu.edu

DOI: 10.1175/JAMC-D-16-0339.1

Antarctic Mesoscale Prediction System (AMPS; e.g., Powers et al. 2012) employs the polar version of the Weather Research and Forecasting (Polar WRF) Model that is primarily developed and maintained by the Polar Meteorology Group at the Byrd Polar and Climate Research Center (Bromwich et al. 2013). The AMPS predictions are primarily utilized by the Space and Naval Warfare Systems Center (SPAWAR), who issue all weather forecasts for USAP. A scarcity of meteorological observing stations and satellite blackout periods that coincide with peak flight times increase the pressure on AMPS for accuracy. Unpredicted fog, low ceilings, and high winds lead to costly failed flight missions, and all are related to the structure of the simulated PBL (A. Cayette 2014, personal communication). Accurately predicting acceptable flight windows is essential to preventing delays in science missions and cargo movement, which lead to additional cost and lost productivity. Developing skill for PBL predictions in forecast models can lead to better representation of the PBL in climate models used to understand the vulnerability of ice sheets to climate change. For instance, an increase in local wind conditions can affect the occurrence and size of polynyas along with coastal deep-water overturning and sea ice formation (Reddy et al. 2007).

The 30-m-tall Alexander Tall Tower! (ATT) on the Ross Ice Shelf provides an important dataset for testing the accuracy of the PBL simulated by Polar WRF. Unlike radiosondes, dropsondes, and single-level automatic weather stations (AWSs), the ATT provides detailed vertical measurements over many years with high temporal resolution (Lazzara et al. 2011). However, the 30-m height of the ATT can only capture the lower PBL behavior, leaving questions about the dynamics throughout the entire depth of the PBL. Wille et al. (2016) focused on the AMPS PBL performance in comparison with 10-min ATT data from 2011 to 2012 to examine the AMPS PBL predictions. The study indicated errors in moisture prediction and handling atmospheric stability as a function of wind speed. AMPS had around a 10-percentage-point dry bias, with slightly drier conditions during winter. The AMPS forecast moisture parameters are generally accurate when compared against radiosonde data at McMurdo and the South Pole (Bromwich et al. 2005; Fogt and Bromwich 2008; Vázquez B. and Grejner-Brzezinska 2013), but the ATT data showed a consistent AMPS dry bias on the Ross Ice Shelf. The dry bias is most evident when the solar elevation angle is lowest in the evening hours, which is when the katabatic flow is strongest (Mather and Miller 1967). The dry bias is also high when winds from the direction of Byrd and Mulock Glaciers exceeded $15\,m\,s^{-1}$, which indicates the dry bias is related to the katabatic flow advecting dry air down through the Transantarctic Mountains. During periods of stable stratification, the ATT climatology showed that AMPS overestimated the wind speed, which slows the development of the temperature inversion in the lower PBL. In this study, an inversion is defined as a layer where temperature increases with height until reaching a maximum, which represents the top of the stable boundary layer.

Throughout the 1-yr study period in Wille et al. (2016), AMPS overestimated the wind speed at the ATT site by $1–2\,m\,s^{-1}$ during all seasons. These results are similar to previous studies that attribute the high wind speed bias to the Mellor–Yamada–Janjić (MYJ) scheme (Hines and Bromwich 2008; Tastula et al. 2012; Bromwich et al. 2013; Valkonen et al. 2014). The study also highlighted the need for observations above the 30-m ATT to measure the depth of the observed dry bias and how PBL stability–wind speed relationship changes throughout the PBL.

AMPS is known to underestimate low-cloud coverage over the Antarctic continent, which is a persistent problem for most models in cold climates (Guo et al. 2003; Fogt and Bromwich 2008; Bromwich et al. 2013). The cloud fraction product in AMPS is so unreliable that most forecasters rely more on AMPS relative humidity as a proxy for cloud predictions (Pon 2015). The cloud fraction product in AMPS is calculated using the cloud liquid water path and cloud ice water path (Fogt and Bromwich 2008). The cold temperatures over the interior of Antarctica lead to very small values for liquid water and ice path, making the cloud fraction very sensitive to small errors in the mixing ratio (Guo et al. 2003). This reliance on AMPS relative humidity for cloud forecasts is concerning when Wille et al. (2016) detected sizable relative humidity errors. While the ATT highlighted the dry bias near the surface, measurements in the critical flight heights of 100–200 m are essential to determine if the AMPS dry bias extends to the heights where low clouds are typically found over the Antarctic ice sheet. In addition, a synoptic analysis of moisture advection over the Ross Ice Shelf would be useful to address questions about the source of the dry bias at the ATT site.

This study utilizes PBL data collected by Small Unmanned Meteorological Observer (SUMO) unmanned aerial systems (UASs) from 13 to 26 January 2014 at the ATT site (Cassano 2014). Continuing the motivation from the previous AMPS PBL study, this analysis examines the performance of AMPS within the PBL in regards to stability and moisture with particular emphasis on how the results from Wille et al. (2016) extend

beyond the 30-m ATT. For the study period, the SUMO UAS flights, ATT data, and European Centre for Medium-Range Weather Forecasts interim reanalysis (ERAI; Dee et al. 2011) data are compared against forecasts from AMPS over the Ross Ice Shelf.

2. Ross Ice Shelf synoptic and mesoscale features

The higher vertical extent of the SUMO UASs along with the greater spatial coverage provided by the ERAI provides a clearer look at the various synoptic features present over the region. Figure 1 displays the various geographical features that shape weather patterns over the Ross Ice Shelf. The meteorological conditions over the Ross Ice Shelf are primarily influenced by a semipermanent wind regime known as the Ross Ice Shelf airstream (RAS). This pressure gradient force (PGF)-driven flow is characterized by the mass transport of negatively buoyant air from the colder Antarctic Plateau across the Ross Ice Shelf via multiple mechanisms (Steinhoff et al. 2009). In the RAS event analyzed by Steinhoff et al. (2009), the katabatic wind flowing down the Transantarctic Mountains combined with marine air from the Ross Sea and orographic ascent over the Queen Maud Mountains to create a stream of low-level clouds that extended across the Ross Ice Shelf. MODIS imagery revealed these cloud streams have a warm signature relative to their surrounding environment despite originating from a colder continental air mass farther inland. RAS events are present over the Ross Ice Shelf about 34% of the time although are less common during the summer (Nigro and Cassano 2014).

Katabatic flow from Byrd Glacier and the surrounding smaller glaciers is one example of a RAS event. The glaciers along the Transantarctic Mountains serve as drainage locations for the katabatic flow from the East Antarctic ice sheet. The Byrd Glacier contributes most of the katabatic flow at the ATT site given the large mass fluxes emerging from the glacier and proximity to the tower (Parish and Bromwich 2007). The position of synoptic lows over the Ross Sea can influence the direction and strength of the katabatic flow coming down the glacier. Relatively warmer air from the Ross Sea with colder katabatic flow draining off Byrd Glacier forms a region of baroclinicity near the mountain base. The baroclinic zone along with the cyclonic vorticity generated from the katabatic wind leads to mesoscale cyclogenesis southeast of Byrd Glacier, which potentially influences snowfall patterns at the ATT site (Carrasco and Bromwich 1991, 1994).

The Transantarctic Mountains serve as barrier for the katabatic winds from West Antarctica, which helps

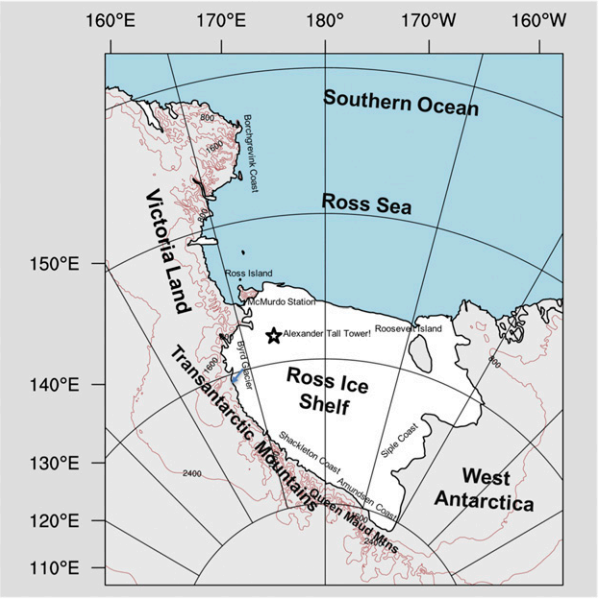

FIG. 1. Map of important geographic features around the Ross Ice Shelf region. The location of the ATT is indicated by the star.

create a confluence zone along the more relaxed slope of the Siple Coast on the eastern Ross Ice Shelf, leading to a RAS event. The low elevation allows low pressure over the South Pacific Ocean to enhance the PGF over the Siple Coast, thus enhancing the katabatic flow that originates over Antarctic interior. The PGF associated with the barrier for the katabatic winds, the downslope buoyancy force, and the enhanced PGF from the semipermanent low over the South Pacific Ocean compose the three forces that enhance the geostrophic wind along the Siple Coast confluence zone (Liu and Bromwich 1997). When this setup is present, the PGF supports katabatic airflow across the Ross Ice Shelf that eventually reaches the ATT site.

A RAS oriented along the base of the Transantarctic Mountains can be an example of a barrier wind jet. Nigro et al. (2012b) conducted a case study of a barrier wind corner jet off the coast of the Queen Maud Mountains. The barrier winds along the Transantarctic Mountains occur when cyclonically driven flow from the Ross Sea pushes stable air into the base of the mountains. Because the boundary layer is often highly statically stable, with the Froude number of the incoming flow frequently less than one, the mountains cause the air to converge along the base instead of flowing over. This mass convergence creates an area of higher pressure along the base while the pressure remains relatively low away from the mountains. The resulting PGF is directed away from the mountains while the Coriolis force deflects the flow westward along the mountain base in

accordance with the geostrophic balance. Surface winds in a barrier wind jet range between 15 and 30 m s^{-1} (O'Connor et al. 1994; Nigro et al. 2012b). Many of the aforementioned weather patterns like the barrier jet were observed during the SUMO field campaign.

3. Polar WRF and ERA-Interim

Continuing from previous work at the ATT site, this study uses the AMPS polar-modified WRF developed by the Byrd Polar and Climate Research Center and the National Center for Atmospheric Research (NCAR). The performance of these modified models has been assessed in the Arctic and Antarctic (Hines and Bromwich 2008; Powers 2009; Bromwich et al. 2009; Hines et al. 2011; Cassano et al. 2011; Bromwich et al. 2013; Hines et al. 2015; Hines and Bromwich 2017). This study utilizes Polar WRF, version 3.3.1, which is an upgrade from Polar WRF, version 3.2.1, used in Wille et al. (2016). Most of the model physics options remain the same as AMPS still utilizes the MYJ PBL scheme with nonsingular implementation of level-2.5 Mellor–Yamada closure for turbulence in the PBL and free atmosphere (Janjić 1994). The surface physics use the same 4-layer Noah land surface model (LSM) with polar modifications (Tewari et al. 2004; Bromwich et al. 2009; Hines et al. 2015). The other physics options such as the Goddard shortwave radiation scheme, Rapid Radiative Transfer Model for GCMs (RRTMG) longwave radiation scheme, and the WRF single-moment (WSM) 5-class microphysics scheme are discussed in further detail in Wille et al. (2016; Antarctic Mesoscale Prediction System 2015).

The analysis presented here is conducted two years after the initial ATT testing from Wille et al. (2016), so higher model resolutions are employed. The earlier analysis utilized 5-km (157 × 190 grid points) domain 3 data, while this study uses the same domain, but the resolution increases to 3 km (538 × 526 grid points; Antarctic Mesoscale Prediction System 2015). This study employs the same 12-h spinup as recommended by previous literature to allow PBL conditions to become quasi steady (Parish and Waight 1987; Parish and Cassano 2003). The AMPS forecast hours used to compare against the SUMO flights all fall within the 12–23-forecast-hour range.

The synoptic analysis of the Ross Ice Shelf uses AMPS Polar WRF domain 3 vertically interpolated to specific pressure levels and ERAI data for model evaluation. The ERA-Interim is a global climate reanalysis that has an ~80-km resolution with 60 vertical levels and provides 6-hourly atmospheric data on fields like temperature, geopotential, relative humidity, and wind. ERAI performs a blend of short-term model simulations with continuous historical observations ingested into a data simulation scheme every six hours as opposed to AMPS, which is a short-term forecast that only uses observations for initialization. One drawback in comparing ERAI against AMPS is that AMPS has a higher horizontal resolution than ERAI, allowing for a better resolution of mesoscale features such as mesoscale vortices and katabatic drainage. In addition, the scarcity of observational data over Antarctica slightly lowers confidence in the ERAI output.

4. SUMO UAS and ATT

Researchers from the Cooperative Institute for Research in Environmental Sciences (CIRES) traveled to the ATT site from 13 to 26 January 2014 to conduct a field experiment using aerial SUMO vehicles to collect atmospheric boundary layer measurements. The figures described later in the results section use UTC to describe time, which is 13 h behind the local time, New Zealand daylight time (NZDT) while the dates on the figure headers are with respect to local time. January is austral summer over Antarctica, where solar noon occurs around 1400 NZDT (0100 UTC) at the ATT site with the sun remaining above the horizon all day. The surface temperatures during the study period ranged from −15° to −4°C.

The SUMO UASs are small, with a 0.8-m wingspan, and weigh 580 g. The aircraft use a Paparazzi open source autopilot system and have an electric engine powered by a rechargeable lithium polymer battery (Mayer et al. 2012; Cassano 2014). Temperature and relative humidity are measured using a Pt Sensiron SHT 75. The temperature accuracy is ±0.3 K with a range from −40° to +124°C and a humidity accuracy of ±2% (Cassano 2014). Vector wind is derived using a no-flow-sensor method and calculated using Eqs. (1)–(3) described below (Mayer et al. 2012).

Over the course of 14 days, the CIRES team conducted 41 flights. After manual quality control, data from 36 flights were chosen for this study. The flight timetable and maximum flight height achieved are listed in Table 1. A typical flight plan involved first calibrating the SUMO UAS in a tent and then walking it outside for launch. After the launch, the UAS would climb to ~30 m and complete an ~140-m diameter circle adjacent to the top of the ATT. Then the UAS would climb to ~100 m and complete another ~140-m diameter circle. The UAS would then repeat this in 100-m intervals ideally up to ~800 m and return to the ground. A typical flight would take between 10 and 20 min. Meteorological conditions on the Ross Ice Shelf sometimes limited the performance of the UASs. The UASs were typically

TABLE 1. The SUMO UAS flight record from the field campaign at the ATT site. Not all flights flown during the field campaign were utilized because of data quality issues.

Flight no.	Starting flight time and date	Max flight height (m)
1	1344 NZDT (0044 UTC) 16 Jan	414
2	1617 NZDT (0317 UTC) 16 Jan	536
3	1225 NZDT (2325 UTC) 17 Jan	523
4	1336 NZDT (0036 UTC) 17 Jan	251
5	1437 NZDT (0137 UTC) 17 Jan	734
6	1619 NZDT (0319 UTC) 17 Jan	654
7	1138 NZDT (2238 UTC) 18 Jan	614
8	1255 NZDT (2355 UTC) 18 Jan	714
9	1427 NZDT (0127 UTC) 19 Jan	807
10	1541 NZDT (0241 UTC) 19 Jan	620
11	1714 NZDT (0413 UTC) 19 Jan	411
12	0925 NZDT (2025 UTC) 21 Jan	319
13	1025 NZDT (2123 UTC) 21 Jan	709
14	1051 NZDT (2151 UTC) 21 Jan	613
15	1215 NZDT (2315 UTC) 21 Jan	590
16	1341 NZDT (0041 UTC) 21 Jan	787
17	1512 NZDT (0212 UTC) 21 Jan	599
18	1641 NZDT (0341 UTC) 21 Jan	515
19	1805 NZDT (0505 UTC) 21 Jan	591
20	1938 NZDT (0638 UTC) 21 Jan	405
21	2109 NZDT (0809 UTC) 21 Jan	399
22	2253 NZDT (0953 UTC) 21 Jan	486
23	1335 NZDT (0035 UTC) 22 Jan	285
24	1021 NZDT (2121 UTC) 23 Jan	689
25	1221 NZDT (2321 UTC) 23 Jan	614
26	1421 NZDT (0121 UTC) 23 Jan	497
27	1727 NZDT (0427 UTC) 23 Jan	688
28	1927 NZDT (0627 UTC) 23 Jan	492
29	0933 NZDT (2033 UTC) 24 Jan	504
30	1059 NZDT (2159 UTC) 24 Jan	689
31	1225 NZDT (2325 UTC) 24 Jan	604
32	1357 NZDT (0057 UTC) 24 Jan	593
33	1533 NZDT (0233 UTC) 24 Jan	725
34	1659 NZDT (0359 UTC) 24 Jan	392
35	1817 NZDT (0517 UTC) 24 Jan	192
36	2145 NZDT (0845 UTC) 24 Jan	692

directed away from clouds to avoid icing issues. Also, the UASs were unable to fly in wind speeds greater than $15\,m\,s^{-1}$, which limited observations during intense katabatic flow events.

Cassano (2014) notes a time lag in temperature and relative humidity measurements with the SUMO, but flying the UAS in a circle at constant height reduces these time lag errors by allowing the sensors to equilibrate with the ambient conditions. This is especially helpful for relative humidity, which for this study is only utilized at the end of each flight circle. Wind speed and wind direction are calculated from data collected while the SUMO UAS flies a circle. The height and location of the SUMO are tracked by GPS every 0.5 s, so a circle within a flight is defined as a period of time where the change in height between individual measurements is less than 4 m. When a SUMO UAS is conducting a circle, the equation for wind speed is

$$\mathrm{ws} = [(\mathrm{max\_gs}) - (\mathrm{min\_gs})]/2, \tag{1}$$

where ws is atmospheric wind speed, max_gs is maximum ground speed, and min_gs is minimum ground speed. The equations for wind direction are

$$a = N_{\mathrm{max\_gs}} - N_{\mathrm{min\_gs}}, b = E_{\mathrm{min\_gs}} - E_{\mathrm{max\_gs}}, \quad \text{and}$$
$$\alpha = \mathrm{atan}\left(\frac{a}{b}\right), \quad \text{with} \tag{2}$$
$$\mathrm{wd} = \alpha + 180^{\circ}, \tag{3}$$

where $N_{\mathrm{max\_gs}}$ is the north position of max_gs, $N_{\mathrm{min\_gs}}$ is the north position of the min_gs, $E_{\mathrm{min\_gs}}$ is the east position of the min_gs, $E_{\mathrm{max\_gs}}$ is the east position of the max_gs, and wd is wind direction. For data quality control, only data collected during the ascent of the SUMO UAS are analyzed because of sensor time lag issues (Cassano 2014).

The specifications of the ATT remain the same for the case study period as described in Wille et al. (2016). The tower's location as represented in Fig. 1 is about 160 km south of McMurdo Station. The tower temperature, relative humidity, and pressure are averaged over 1-min intervals, while the wind speed and direction are resultants over 2-min intervals. The averages are taken every 10 min and then quality controlled. Snow depth changes the instrument height above surface, but the changes are generally small enough to not significantly impact the temperature sensors located at 1, 2, 4, 7, 15, and 30 m above the surface. Relative humidity is measured at 7 and 30 m, and wind speed and direction are measured at 4, 7, 15, and 30 m. The ATT is managed by the Antarctic Meteorological Research Center in Madison, Wisconsin, who manually quality control the ATT data to account for any observational errors related to solar heating, frost deposition, and instrument freezing as outlined in Lazzara et al. (2012). The error bars seen in figures discussed later represent standard error of the mean $[\mathrm{sd}/(n)^{1/2}]$, where sd is the standard deviation and n is the number of observations.

5. Results

a. ERA-Interim validation

To determine the accuracy of the spatial plots discussed later in this study where synoptic conditions in AMPS and ERAI are compared against one other, the ERAI data were compared against the independent SUMO UASs observations at the ATT site, which are not assimilated into ERAI. The ERAI data are

composed of 42 analyses at 6-h intervals ranging from 15 to 25 January to represent weather conditions during the study period. The ERAI was vertically interpolated to specific height levels and horizontally interpolated to the ATT location. The ERAI skin temperature and 2-m relative humidity are included in the vertical interpolation to increase data resolution near the surface. Because the ERAI data are produced at 6-h intervals, it is difficult to match the time of the ERAI data against the time of a particular SUMO UAS flight, thus lowering accuracy in the ERAI SUMO comparison. The results show ERAI wind speed is generally within 1 m s^{-1} of the SUMO observations, and wind direction is within 10°. There is an approximate 10-percentage-point dry bias above 100 m in ERAI. However, the ERAI surface to 100-m temperature is around 3°–4°C warmer than the temperatures observed from the SUMO UAS flights. This differs from a previous examination of ERAI over Antarctica that found no significant annual bias in ERAI when compared against three AWSs nearby the ATT from 2002 to 2013, but these data were assimilated (Jones and Lister 2015). By contrast, Jakobson et al. (2012) found that the ERAI temperature analysis had a warm summer bias of up to 2°C in the lowest 400 m over the central Arctic Ocean when compared against nonassimilated tethersonde data.

The ERAI 6-hourly analyses can be directly compared against the corresponding AMPS hourly forecast data. Figure 2 shows the differences between the ERAI simulations and the corresponding AMPS forecasts at the ATT site. On average, ERAI is 3°–4°C warmer near the surface than AMPS, which is similar to the temperature bias found between the SUMO observations and ERAI. The AMPS relative humidity is up to 15 percentage points lower than the reanalysis data, which was already slightly drier than the SUMO observations. Above 100 m, the AMPS wind speed is about 2–3 m s^{-1} higher than ERAI, and the wind direction difference is within the range of standard error at all heights. Because of the large temperature bias found in ERAI, it would be inaccurate to compare the AMPS temperatures against ERAI across the Ross Ice Shelf. Given the warm bias in ERAI and that relative humidity is a function of temperature and moisture, the ERAI relative humidity is not a great benchmark for comparison but can provide further detail in moisture advection and cloud development. The validation shows that ERAI can accurately simulate wind speed and direction at the ATT location.

b. PBL stability

The first goal of the comparison was to investigate if the AMPS near-surface wind speed excess is also found in upper layers and how that affected the PBL stability. When focusing on cases where the SUMO flights document a definite inversion, the impact on stability from overestimated wind speeds becomes clear. During the field campaign, 69% ($n = 25$) of the analyzed SUMO UAS flights recorded an inversion. The corresponding AMPS forecasts simulated 60% ($n = 15$) of the 25 observed inversions from the SUMO flights. There were no cases where AMPS simulated a near-surface inversion when one did not exist according to the SUMO UAS. Figure 3 plots instances where a SUMO flight records an inversion and compares it against the corresponding AMPS forecast. Cases in which AMPS does not simulate an inversion when one is observed are recorded as zero. In 79% ($n = 19$) of observed inversions, AMPS underestimates the inversion strength. AMPS overestimates the wind speed in the inversion layer in 72% ($n = 16$) of the cases in which an inversion is observed and the SUMO UAS performs a flight circle above the inversion layer to measure wind speed. Model vertical resolution certainly impacts the ability of AMPS to resolve the inversion strength; however, overestimated wind speeds appear to drive excessive mechanical mixing in the PBL. This overestimation of wind speed is not limited to cases where an inversion is present. Figure 4 shows that AMPS had a consistent 2–3 m s^{-1} positive bias at all observable levels during the study period, which is consistent with previous studies (Hines and Bromwich 2008; Tastula et al. 2012; Valkonen et al. 2014; Wille et al. 2016).

Looking at the spatial average of wind speeds over the Ross Ice Shelf from AMPS and ERAI (Fig. 5) reveals AMPS has a higher 950-hPa wind speed in a region extending from the northwest Ross Ice Shelf across the Ross Sea compared against ERAI. This region, which includes the ATT site, was influenced by a persistent offshore cyclone. The examination of the mean 950-hPa geopotential height showed that AMPS has a higher average intensity of that offshore cyclone, which increased the pressure gradient across the Ross Sea and led to increased wind speeds at the edge of the Ross Ice Shelf.

c. PBL moisture

The SUMO UASs provided high-resolution moisture observations through the PBL and into the free atmosphere. This allowed for detailed observations at the heights where low clouds typically form over the ice shelf. When all the flight data and corresponding AMPS forecasts are averaged together, a 10-percentage-point dry bias appeared near the surface, which agrees with the tower observations from Wille et al. (2016) (Fig. 6). Above the height of the ATT, the dry bias increased to 25–30 percentage points from 200 to 400 m before

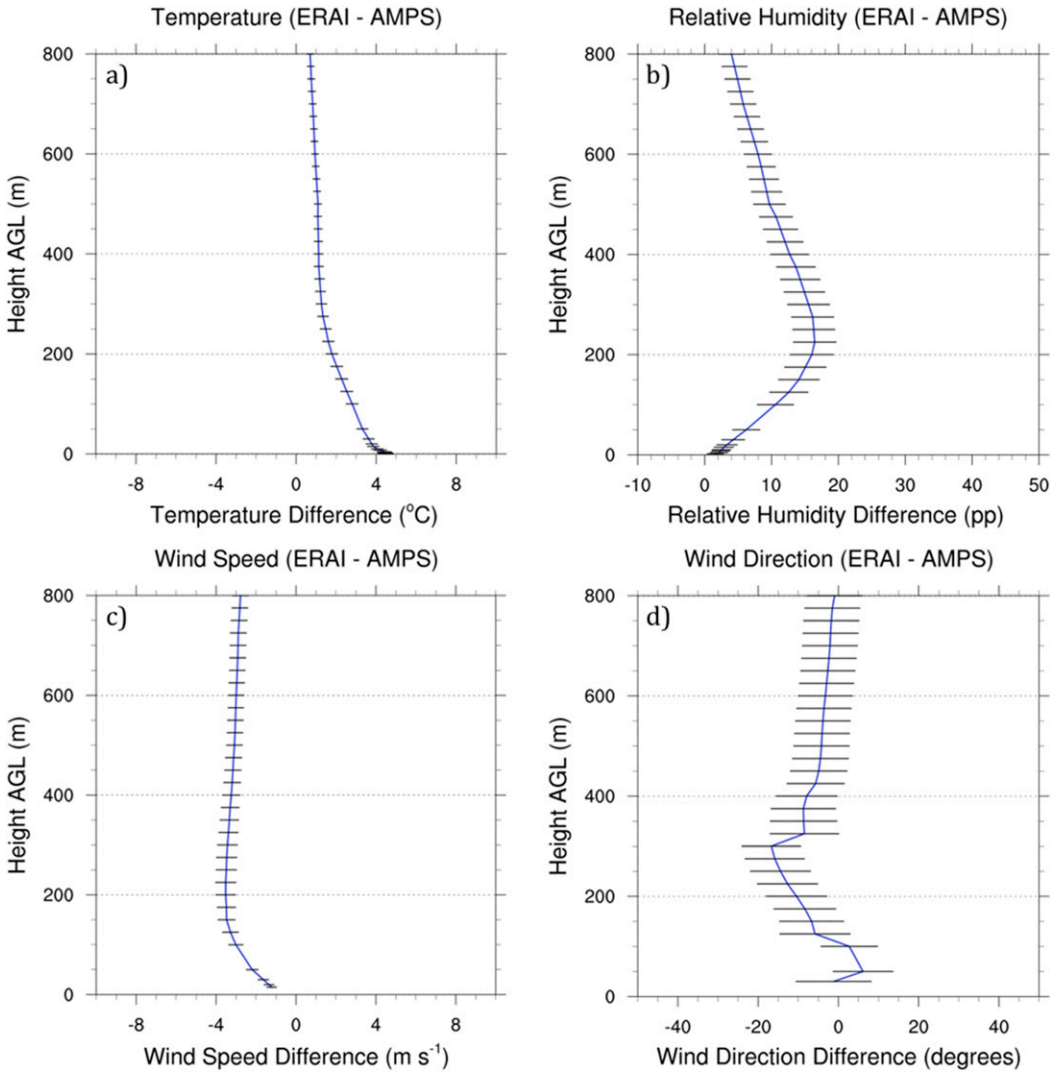

FIG. 2. The (a) mean temperature, (b) relative humidity, (c) wind speed, and (d) wind direction differences between 42 ERAI analyses at 6-h intervals and the corresponding AMPS forecasts from 1200 UTC 15 Jan to 1800 UTC 25 Jan. The differences for all variables are ERAI − AMPS. The error bars represent the standard error of the mean; 360° is added to wind directions between 0° and 100° to avoid wraparound errors.

decreasing back to 10 percentage points around 600 m. The dry bias is equally evident when looking at the specific humidity difference between the SUMO UAS flights and AMPS. Between 200 and 400 m, AMPS had an average 0.8 g kg^{-1} specific humidity deficit. With the confirmation from the specific humidity and AMPS only displaying a ~1°C cold bias throughout the study period (and lack of significant cold biases), the relative humidity errors are certainly related to how AMPS resolves moisture. This significant dry bias is likely related to the low-cloud problems in AMPS.

After examining the ERAI and AMPS relative humidity field on the Ross Ice Shelf, it is evident that the katabatic flow in AMPS advected unrealistically dry air down from the Transantarctic Mountains across the western Ross Ice Shelf and over the ATT site during the field campaign (Fig. 7). According to AMPS, the unrealistically dry air even reached McMurdo Station, thus raising concerns about low-cloud prediction over the nearby airfields. The wind direction bias seen in Fig. 4, and less clearly in Fig. 7, shows that the source of the katabatic winds over the ATT site might have influenced the dry bias. The 10°–20° westward wind direction bias in AMPS means the katabatic wind flowed down glaciers closer to the ATT site, thus reducing the distance the flow travels over the Ross Ice Shelf before reaching the ATT. ERAI had a slight dry bias when compared against the SUMO UAS flights but was more accurate

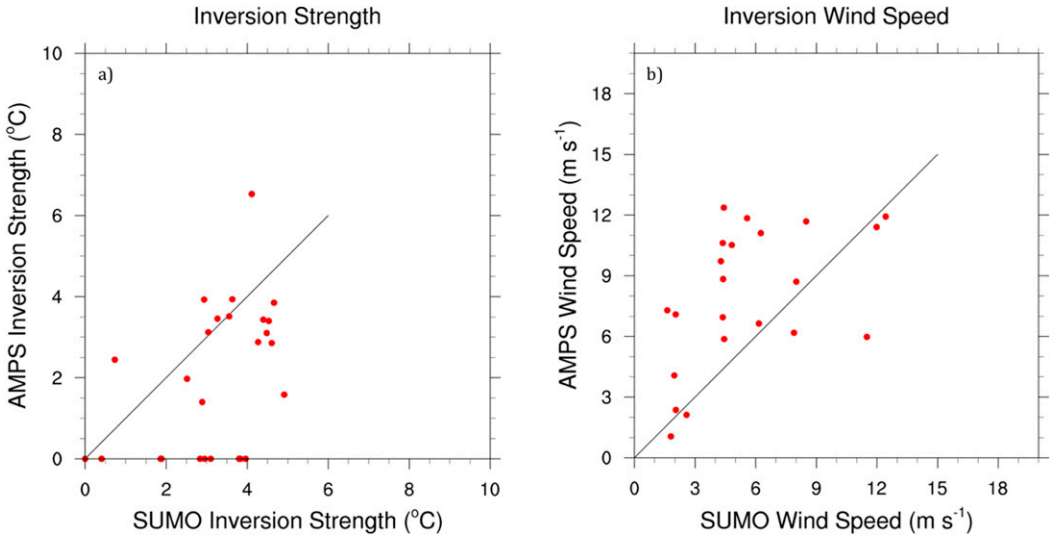

FIG. 3. (a) The SUMO and AMPS inversion strength and (b) the corresponding wind speed at the top of the inversion layer when a temperature inversion is present during a SUMO UAS flight; 25 of the 36 total SUMO flights recorded an inversion. If the corresponding AMPS forecast did not simulate an inversion, the inversion strength is listed as zero. The black line added for perspective corresponds to a perfect match.

than AMPS. The SUMO near-surface relative humidity measurements matched the ATT observations in nearly every flight, thus raising confidence in the tower and SUMO UAS observations.

d. Illustrative case studies

Examining a particular day of the study period reveals finer details about the development of the PBL and how AMPS and ERAI resolve these features. The three days chosen for the case studies (23, 16, and 24 January) add value to analysis of average behavior from this study and Wille et al. (2016) while also showing the complexity of circulation patterns over the Ross Ice Shelf. The 23 January data showed the tendency for AMPS to favor drier katabatic flow and how complex mesoscale cyclones in AMPS are difficult to validate because of the

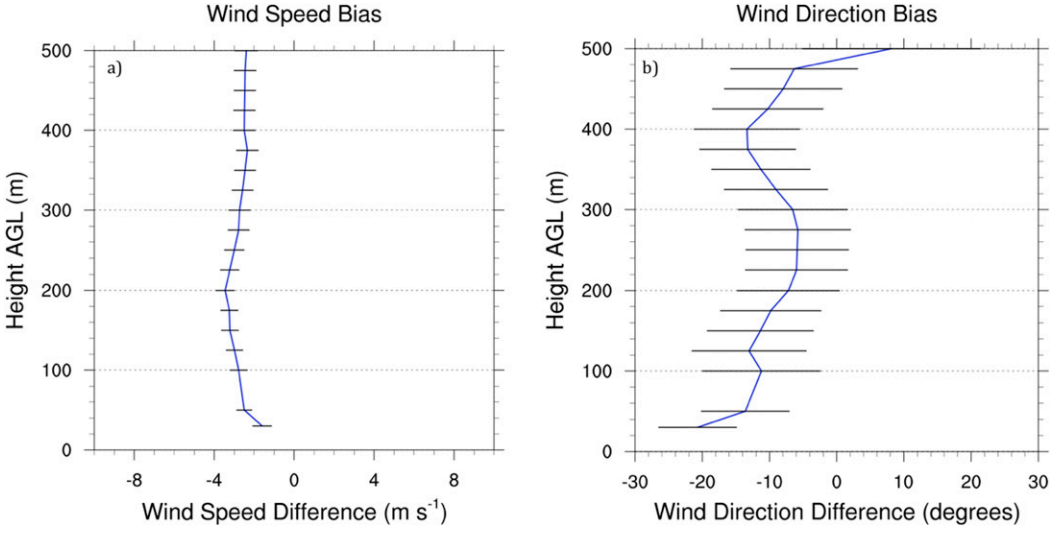

FIG. 4. The mean wind (a) speed and (b) direction differences between the 36 analyzed SUMO flights and the corresponding AMPS forecast where the difference for wind speed and direction is SUMO − AMPS. This means all model biases in the wind direction are westward. The error bars represent standard error of the mean; 360° is added to wind directions between 0° and 100° to avoid wraparound errors.

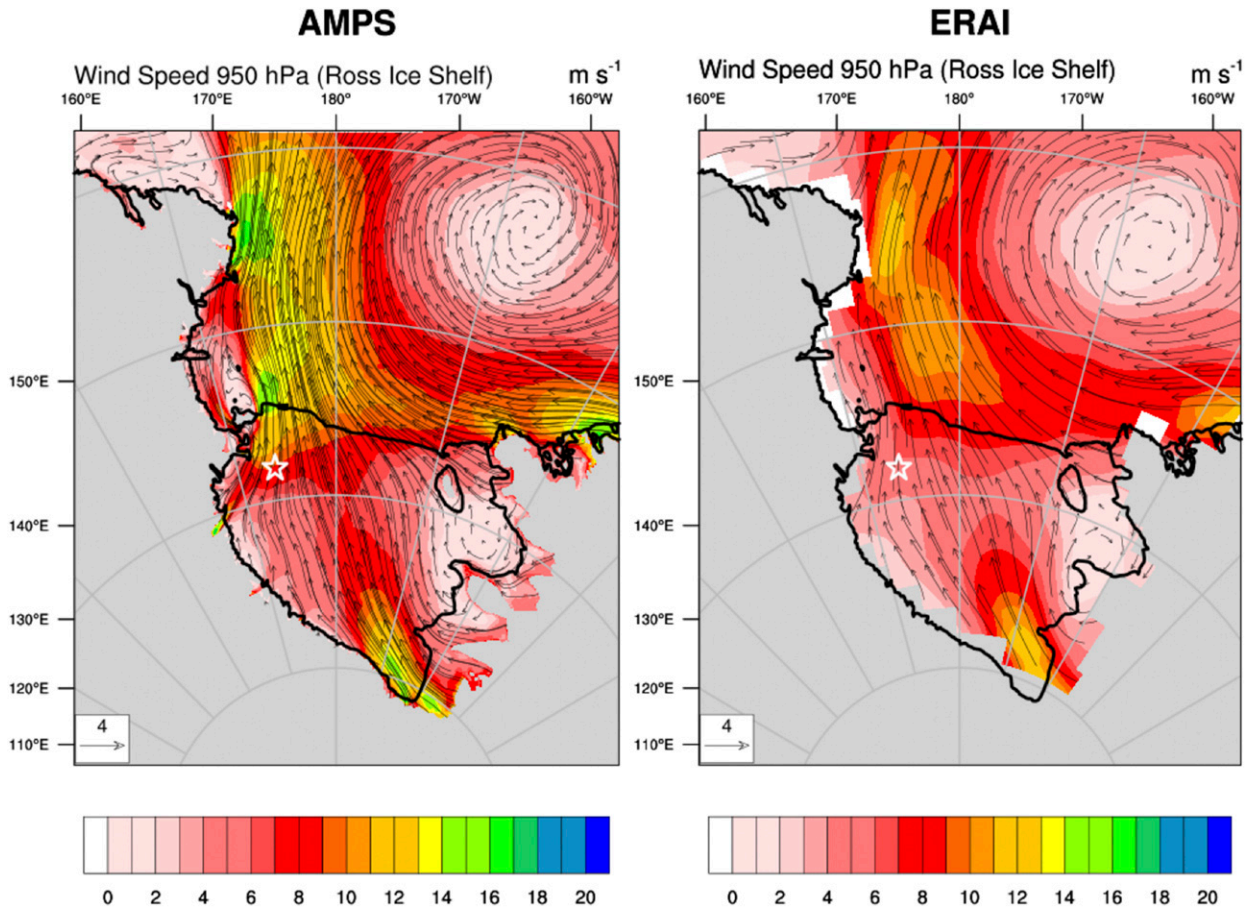

FIG. 5. The 15–25 Jan 950-hPa average wind vectors for (left) AMPS and (right) ERAI. The colors represent the vector average wind speed. The average is composed of 42 ERAI analyses and corresponding AMPS forecasts; 950 hPa is ~300 m above the surface. The star is the location of the ATT.

lower resolution in ERAI. The 16 January data showed how AMPS can simulate unrealistically strong winds and dry air during a katabatic wind regime. The 24 January data highlighted how despite a general agreement in circulation and wind speed, AMPS still underestimated moisture like 16 January. Also, the eight flights on 24 January provided useful information on the development of the PBL throughout the day. All three days along with other days not discussed share a common theme where unrealistically dry air in the AMPS simulations appear related to the advection of dry air from the Antarctic Plateau.

1) 23 JANUARY

On 23 January, there were five SUMO flights around 2100–0600 UTC (1000–1900 NZDT; Table 1). The SUMO observations show light 2–5 m s^{-1} winds that created ideal conditions for a convective boundary layer that was nearly saturated and a sharp 6°C temperature inversion starting at 75 m that gradually weakened throughout the day (Fig. 8). The SUMO flights showed the atmosphere dried past the height of inversion. AMPS relative humidity decreased above the surface, leading to a significant 50-percentage-point dry bias at 200 m above the surface. While AMPS was able to capture the general shape of the inversion, it overestimated the boundary layer thickness by 100 m and underestimated the inversion strength by 3°C. The ATT, SUMO, and ERAI show winds coming from the northwest; however, AMPS maintained a southwest katabatic flow originating from Byrd Glacier. This leads to a 4–6 m s^{-1} positive wind speed bias about 200 m above the surface.

The 950-hPa relative humidity chart in Fig. 9 paints a rather complex circulation picture. At 0000 UTC, AMPS simulated a mesoscale anticyclonic vortex to the north and a mesoscale cyclonic vortex to the south that were likely shear-driven features on the edge of the katabatic flow draining from Byrd Glacier, which extended over the ATT site. The AMPS setup was similar

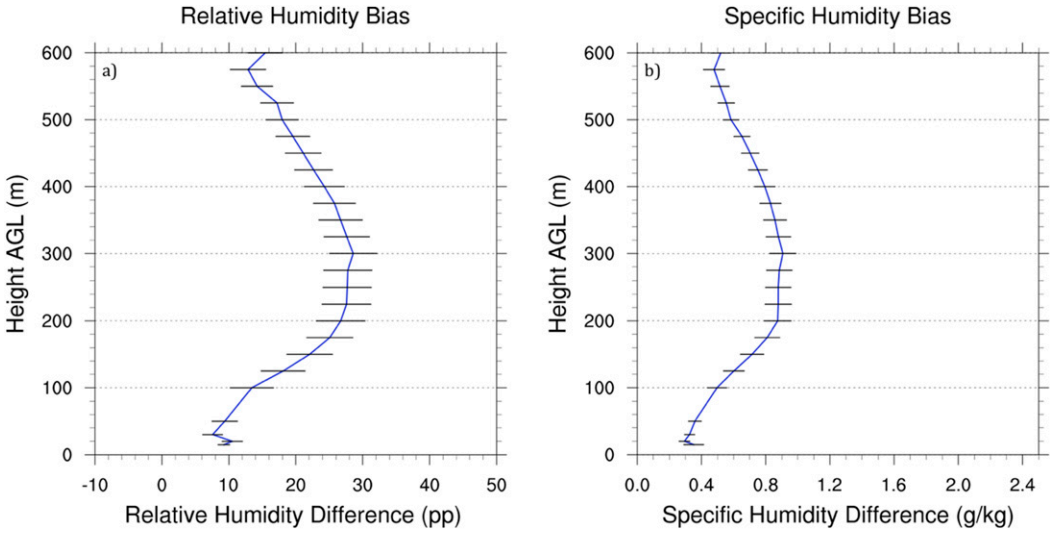

FIG. 6. The (a) relative and (b) specific humidity difference between the 36 analyzed SUMO flights and the corresponding AMPS forecasts where the difference for relative and specific humidity is SUMO − AMPS. The error bars represent standard error of the mean.

to the mesoscale cyclogenesis case described by Carrasco and Bromwich (1991). From the AMPS simulation, the mesoscale circulation would have amplified the katabatic flow over the ATT site, bringing colder and drier air down from the Antarctic Plateau. The stronger winds associated with the katabatic flow would enhance mixing and bring warmer air to the surface while decreasing the average temperature throughout the column (Steinhoff et al. 2009). Although the general agreement in temperature between AMPS and the observations makes it unclear if a strong katabatic wind was present, it is important to note that a small change in the positioning of the mesoscale vortices seen in AMPS would have led to a large difference in conditions at the ATT site. Meanwhile, ERAI agreed with the SUMO wind direction and brought moist air from the Ross Sea over the ATT instead of having katabatic flow from Byrd Glacier. This difference in airmass advection led to AMPS creating drier conditions than shown in SUMO and ERAI. The 950-hPa ERAI relative humidity shows southeastward moist air advection from the coast of Victoria Land. It appears the reason behind the difference in air masses is a difference in a ridge that was significantly more meridionally extended in ERAI than in AMPS, which only had a slight ridge near the Borchgrevink Coast. The ERAI simulation allowed the marine air mass to reach the western Ross Ice Shelf, while katabatic flow dominated in AMPS. Given that ERAI wind direction agrees with the SUMO observations at the ATT site, it is likely that a marine air mass was present over the ATT site as opposed to a katabatic flow as simulated by AMPS. MODIS imagery from the *Aqua* satellite taken at 0500 UTC (not shown) indicated mid- to upper-level clouds in the region of the ATT associated with the ridge. From the satellite imagery, ERAI, and observations, it appears the ridge advected moist air over the ATT site while creating a RAS event over the central Ross Ice Shelf that was evident on the MODIS image as a cloud streak that extended over the Ross Sea. The AMPS circulation errors during 23 January in Fig. 9 were an exception to the norm as AMPS generally did well at simulating the large-scale circulation patterns during the field campaign.

2) 16 JANUARY

The analysis of synoptic conditions on 23 January showed a significant dry bias that was caused by AMPS not properly resolving a ridge that advected relatively moist marine air over the Ross Ice Shelf. The conditions seen on 16 January were more typical of the dry bias seen in the average relative humidity field in Fig. 7. On that day, there were two SUMO flights around 0100 and 0300 UTC (1400 and 1600 NZDT; Table 1). Figure 10 shows the main discrepancies are in the wind speed, relative humidity above 150 m, and temperature with a slight wind direction bias. AMPS simulated the near-surface relative humidity reasonably well but then exhibited a 45-percentage-point dry bias above 200 m. This bias is similar to the average relative humidity bias in Fig. 6. AMPS also simulated the lower-level temperature relatively well but developed a ~2°C warm bias above 200 m. The SUMO wind observations indicated a positive 1–3 m s^{-1} bias in the AMPS wind speed at all vertical levels like the average wind speed bias in Fig. 4.

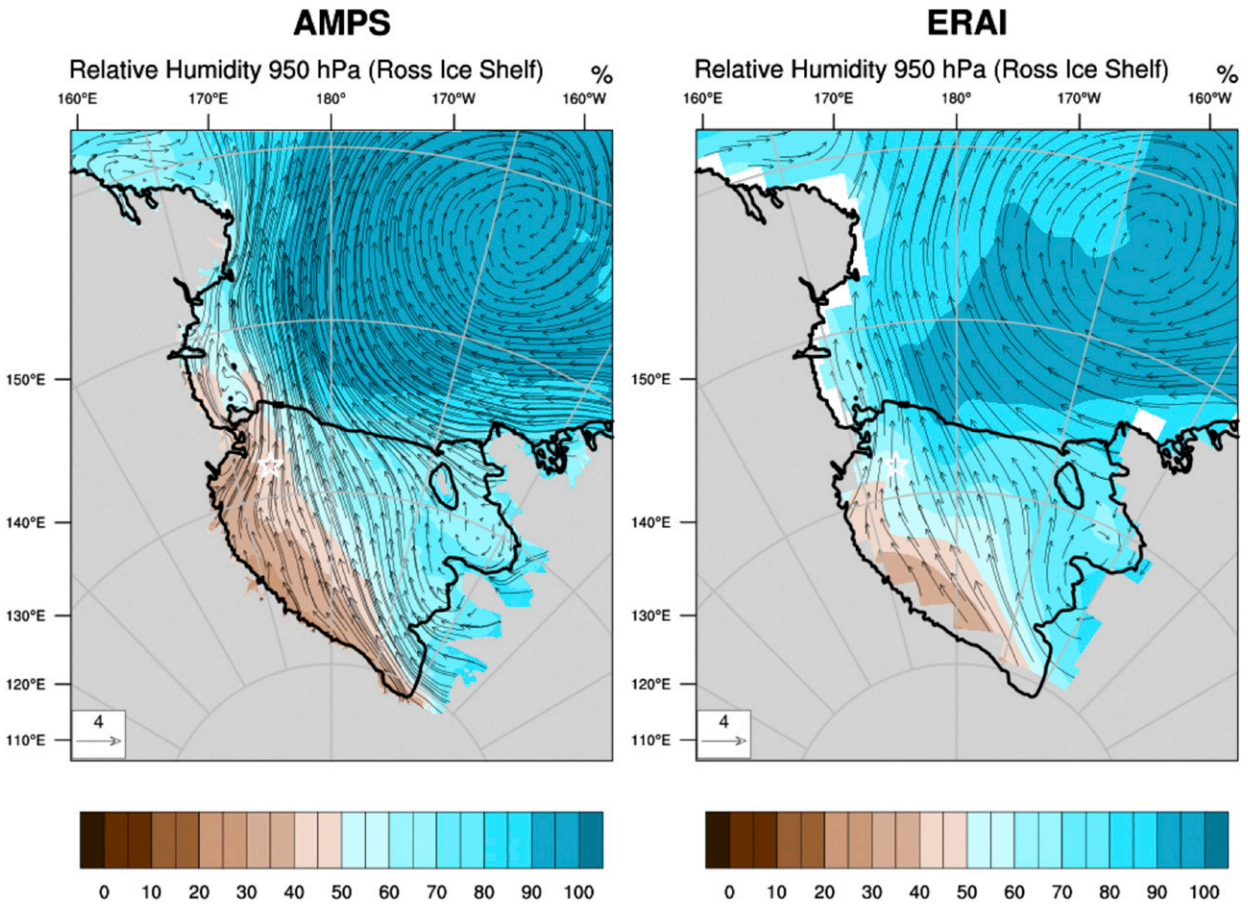

FIG. 7. The 15–25 Jan 950-hPa average relative humidity (colors; percent) and vector wind (arrows; m s^{-1}) for (left) AMPS and (right) ERAI. The average is composed of 42 ERAI analyses and corresponding AMPS forecasts. The star is the location of the ATT.

The observations also showed an ~18° westward wind direction. This difference in wind direction potentially means that the simulated katabatic wind in AMPS is originating from a different glacier, which would affect the relative humidity dry bias.

The synoptic 950-hPa-level wind speeds show that the AMPS's positive wind speed bias may be caused by the origin of the katabatic flow. ERAI data show the katabatic flow traveled a greater distance across the Ross Ice Shelf before reaching the ATT as opposed to AMPS, which had the winds originating from the relatively closer Byrd Glacier. The 950-hPa geopotential heights and relative humidity show the AMPS wind direction was overly influenced by a developing cyclone over the Siple Coast (Fig. 11). This slight deviation in the wind direction between AMPS and ERAI results in drier air being advected down from the Transantarctic Mountains, leading to errors in relative humidity. The AMPS 950-hPa relative humidity shows the ATT site sitting on the edge of a 40-percentage-point relative humidity gradient, possibly indicating that a slight difference in wind direction led to large differences in relative humidity.

3) 24 JANUARY

The 24 January data had relative humidity biases similar to 16 January, where AMPS simulated unrealistically dry air above the near surface. This day has the lightest winds of the case studies and is one of the few days where there was consistent agreement in modeled and observed wind speed. There were eight SUMO flights throughout day from 2000 to 0900 UTC (0900–2200 NZDT; Table 1). During the 2000–0100 UTC flights, the near-surface relative humidity bias in AMPS is around 10 percentage points (Fig. 12). That bias increased to around 50 percentage points at 200 m. Between 150 and 300 m, the 0000 UTC ERAI had a relative humidity bias of around 5–15 percentage points but is accurate at all other heights. During the afternoon, the observed moist layer extended to 300 m, and AMPS maintained a 50-percentage-point dry bias

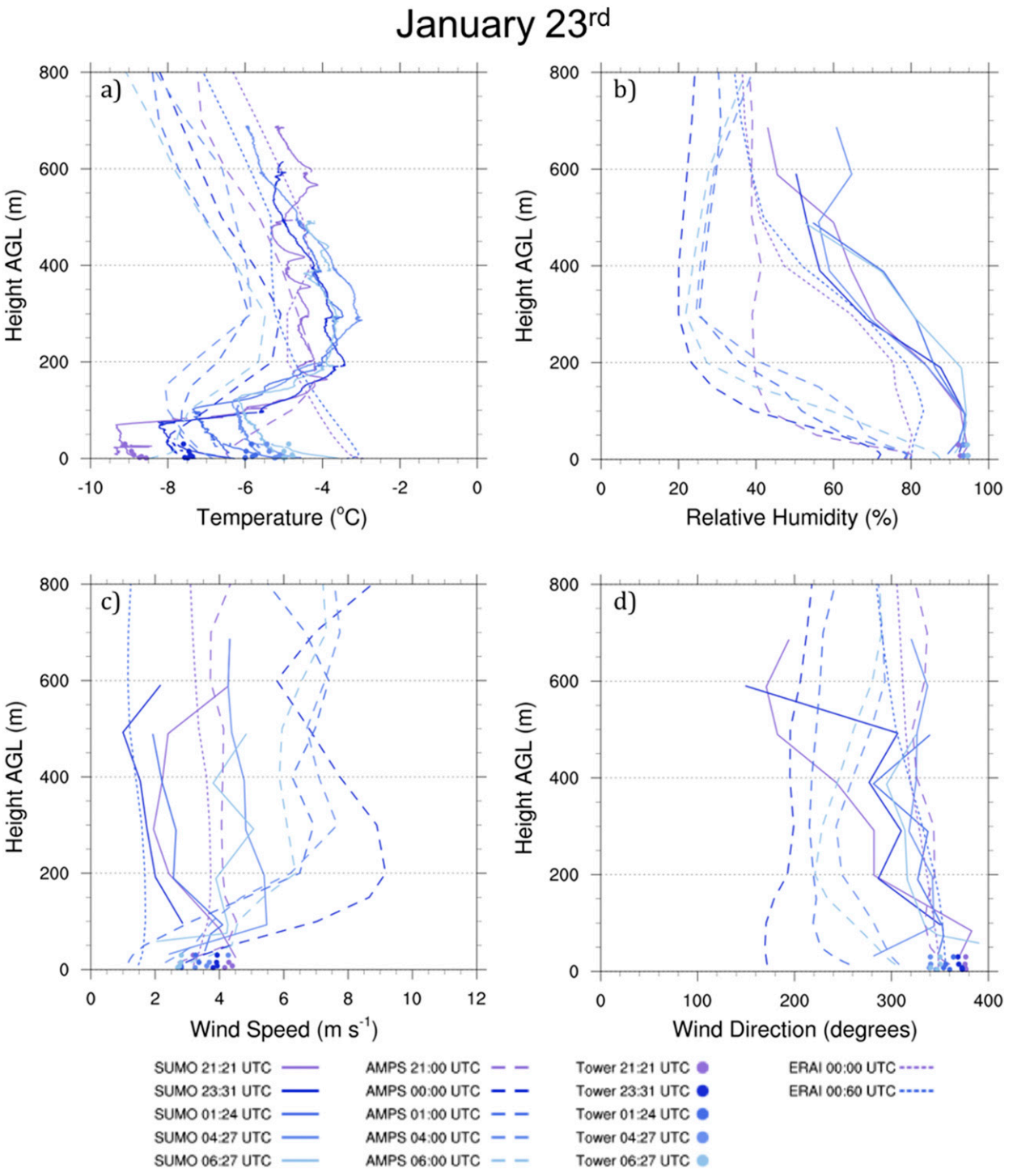

FIG. 8. The 23 Jan SUMO (solid lines), AMPS (long dashed lines), ERAI (short dashed lines), and ATT (solid circles) data for (a) temperature, (b) relative humidity, (c) wind speed, and (d) wind direction; 360° is added to wind directions between 0° and 100° to avoid wraparound errors.

(Fig. 13). The surface winds range from 1 to 4 m s^{-1} throughout the day in the observations and AMPS simulations, which led to radiative cooling at the ice surface. AMPS accurately captured the low-level temperatures in the morning, but the radiational cooling became excessive during the 0900 UTC simulation, with a 7°C cold

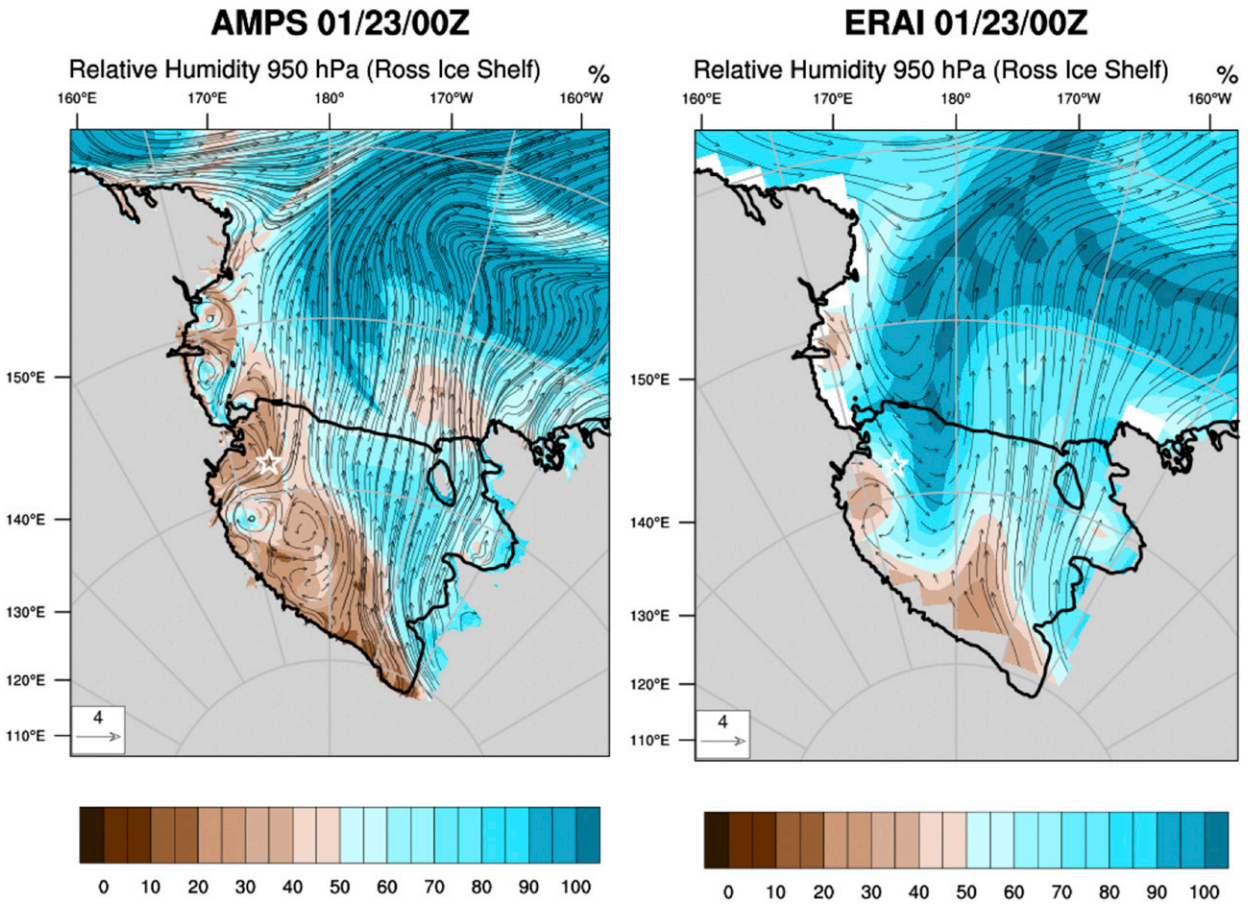

FIG. 9. The 0000 UTC 23 Jan 950-hPa relative humidity (colors; percent) and vector wind (arrows; $m\,s^{-1}$) for (left) AMPS and (right) ERAI. The star is the location of the ATT.

bias at the surface (Fig. 13). When looking at a time series for the evolution of the PBL in AMPS and the observations, the AMPS inversion strength is 1°–2°C less than the observed inversion strength during the first three flights in the morning. The bias becomes less significant by the fourth flight, around 0100 UTC. There appear to be no significant differences in the PBL height.

The 950-hPa vector wind speed at 0000 UTC indicates mesoscale vortices that might be responsible for the 30° westward wind direction bias in AMPS. The ERAI lacks the resolution to resolve mesoscale vortices, and Nigro et al. (2012a) showed AMPS resolves about 40% of observed cyclone activity in a region extending from Byrd Glacier to Terra Nova Bay. Therefore, it is difficult to determine whether the vortices simulated by AMPS are realistic. Nevertheless, AMPS generated an anticyclonic vortex to the east of the ATT and a cyclonic vortex off to the south. AMPS had a continental air mass over almost the entire ice shelf, while ERAI displayed a moister layer over the northwest Ross Ice Shelf (Fig. 14). The 950-hPa geopotential height and vector wind speed suggest that a cyclone over the Siple Coast was stronger in AMPS than in the reanalysis, which enhanced the katabatic flow over the Siple Coast in AMPS. In addition, the mesolow and mesohigh couplet near the ATT simulated in AMPS interacted with the cyclone over the Siple Coast to direct the katabatic flow with winds exceeding $20\,m\,s^{-1}$ north of the Amundsen Coast. The mesolow also steered the katabatic flow from Byrd Glacier to the ATT site. Since ERAI did not resolve the mesovortices on the western Ross Ice Shelf, the wind flow appears more diffluent near the ATT site with a weaker katabatic flow.

6. Discussion

From the combined multiyear near-surface PBL analysis of the ATT (Wille et al. 2016) and the present SUMO UAS summer field campaign that provided detailed boundary layer observations up to 800 m, there is a comprehensive record of PBL behavior over the

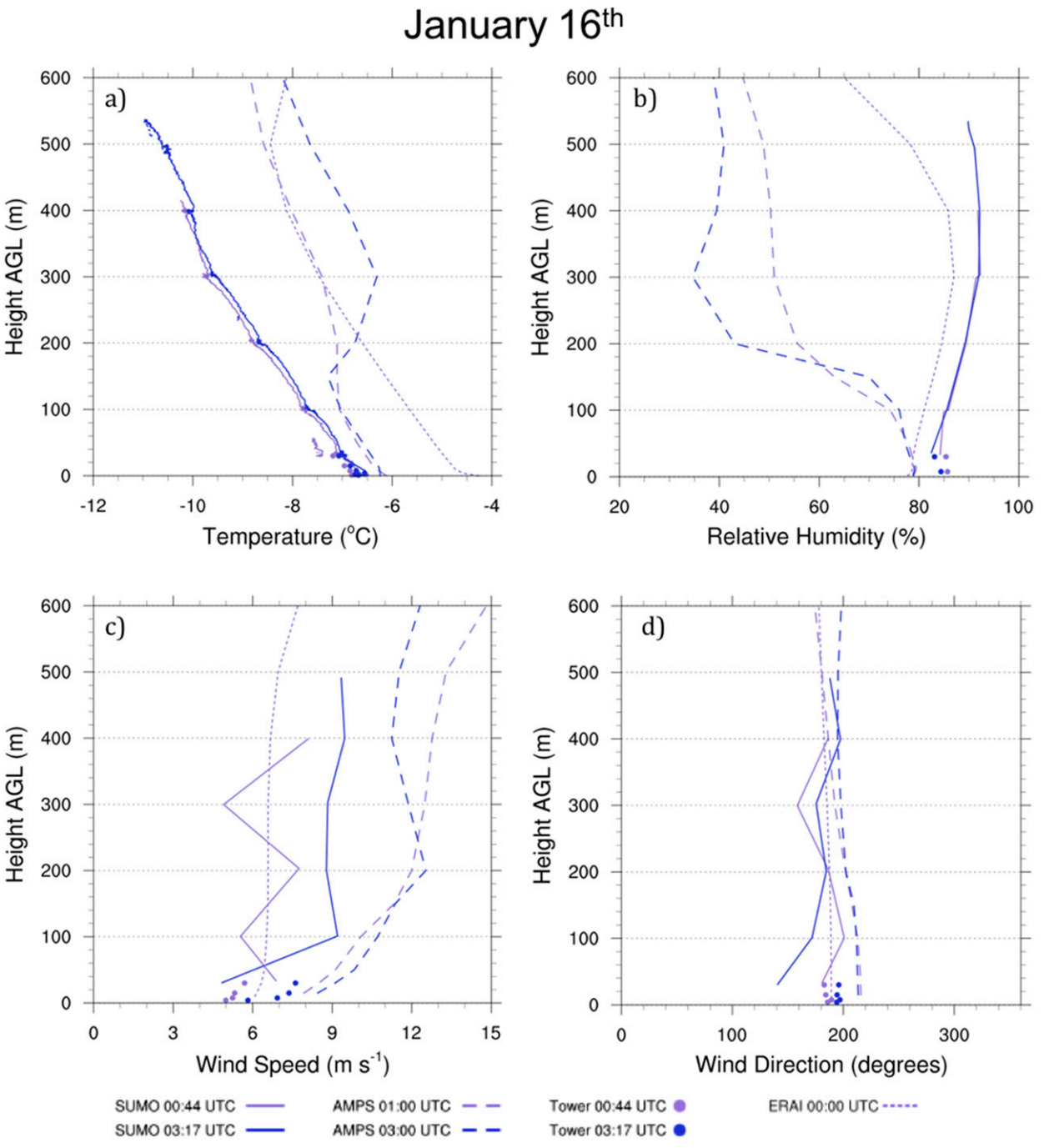

FIG. 10. The 16 Jan SUMO (solid lines), AMPS (long dashed lines), ERAI (short dashed lines), and ATT (solid circles) data for (a) temperature, (b) relative humidity, (c) wind speed, and (d) wind direction.

Ross Ice Shelf that can be compared against the performance of AMPS. The multiyear evaluation of the AMPS PBL simulations at the ATT site revealed that AMPS persistently underestimated the relative humidity from 10 to 15 percentage points and simulated excessive mechanical mixing in the lower PBL. The similar observations from the ATT and the SUMO UASs during the field campaign raise confidence in both the results from the previous study and the accuracy of the UAS beyond the height of the ATT. The results from this study show that many of the biases first noted in Wille et al. (2016) are seen again through the depth of the PBL and in many cases are larger above the height of the ATT. Given the agreement in low-level results about

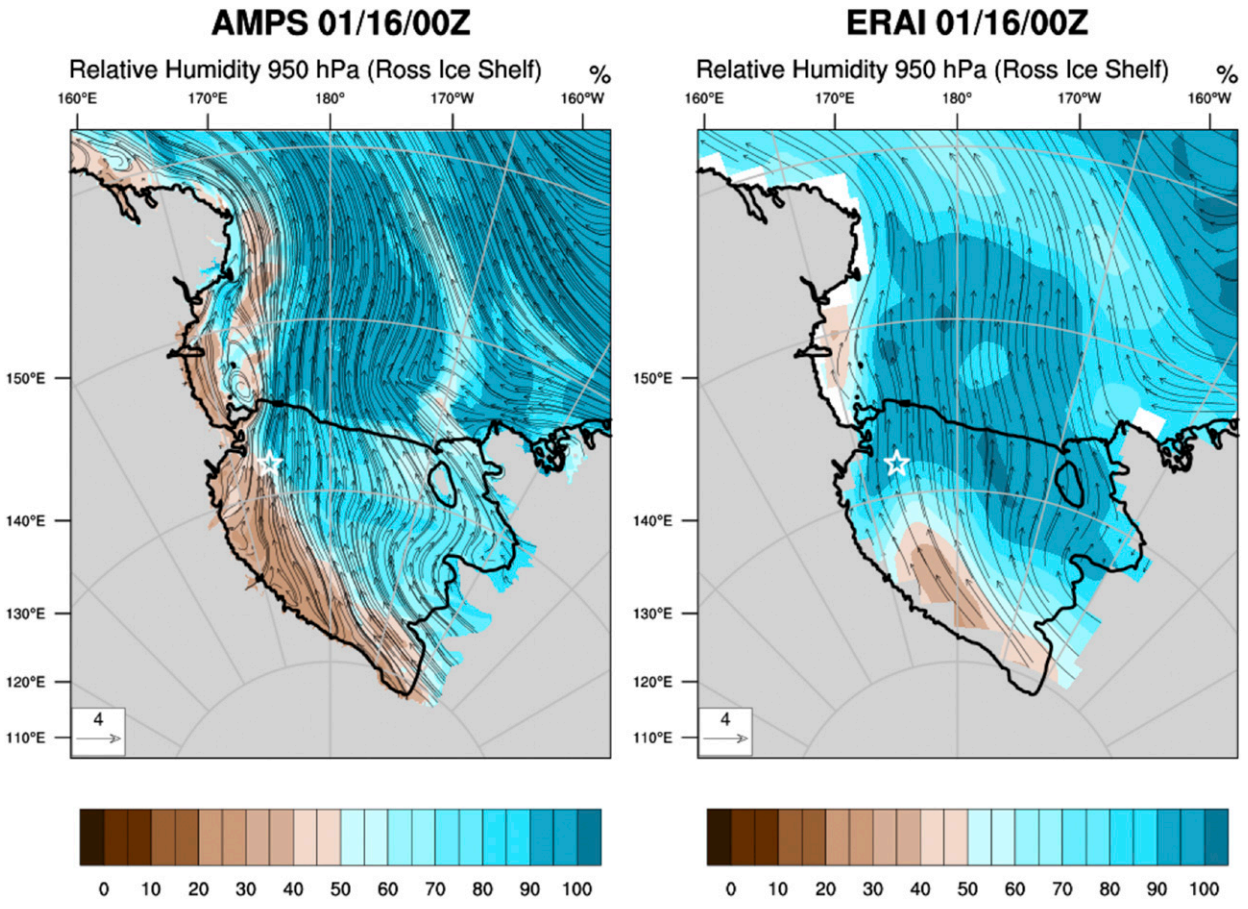

FIG. 11. As in Fig. 9, but for 0000 UTC 16 Jan.

the AMPS biases between this two-week summer field campaign and in Wille et al. (2016), it is likely that the biases seen throughout the rest of the PBL in this study occur regularly over the ATT site and the Ross Ice Shelf regardless of the season.

In the previous study, AMPS had a 1–2 m s^{-1} wind speed bias compared against the ATT. In this study, the bias slightly increases to 2–3 m s^{-1} above the height of the ATT up to 800 m. During conditions when an inversion was present, AMPS underestimated the inversion strength 76% of the time. Even during the summer, atmospheric inversions are a common feature on the Ross Ice Shelf. They occurred during 69% of SUMO UAS flights but were only detected in 42% of AMPS simulations. On two days (19 and 23 January), there were biases in the depth of the boundary layer. In each case, AMPS underestimated the intensity of the inversion and overestimated the boundary layer depth by 100 m. This study did not explicitly examine the MYJ scheme in AMPS, but previous studies show a similar high wind speed bias over Antarctica when focusing on the PBL scheme (Hines and Bromwich 2008; Tastula et al. 2012; Bromwich et al. 2013; Valkonen et al. 2014). As a result, AMPS overestimates the mechanical mixing within the PBL, thus unrealistically underestimating the stability.

Past the height of the ATT, the relative humidity biases increased significantly from the 10–15-percentage-point bias seen in Wille et al. (2016). The SUMO UASs confirmed similar biases near the height of the ATT but then increased to around 25–30 percentage points from 200 to 400 m. A similar pattern is seen in the calculated specific humidity, verifying that there is indeed a dry bias in AMPS. Because of flight restrictions during periods of high winds and a limited temporal dataset, it is difficult to discern how the dry bias changes with wind speed. The ERAI data provided an overview of synoptic conditions over the Ross Ice Shelf during the study period. While the moisture biases are sometimes related to cyclone positioning errors in AMPS that changed the source of the moisture advection, the majority of the errors stem from unrealistically dry air being advected by the katabatic flow. Figure 7 shows that AMPS and ERAI have similar mean vector wind fields throughout the study period, but AMPS

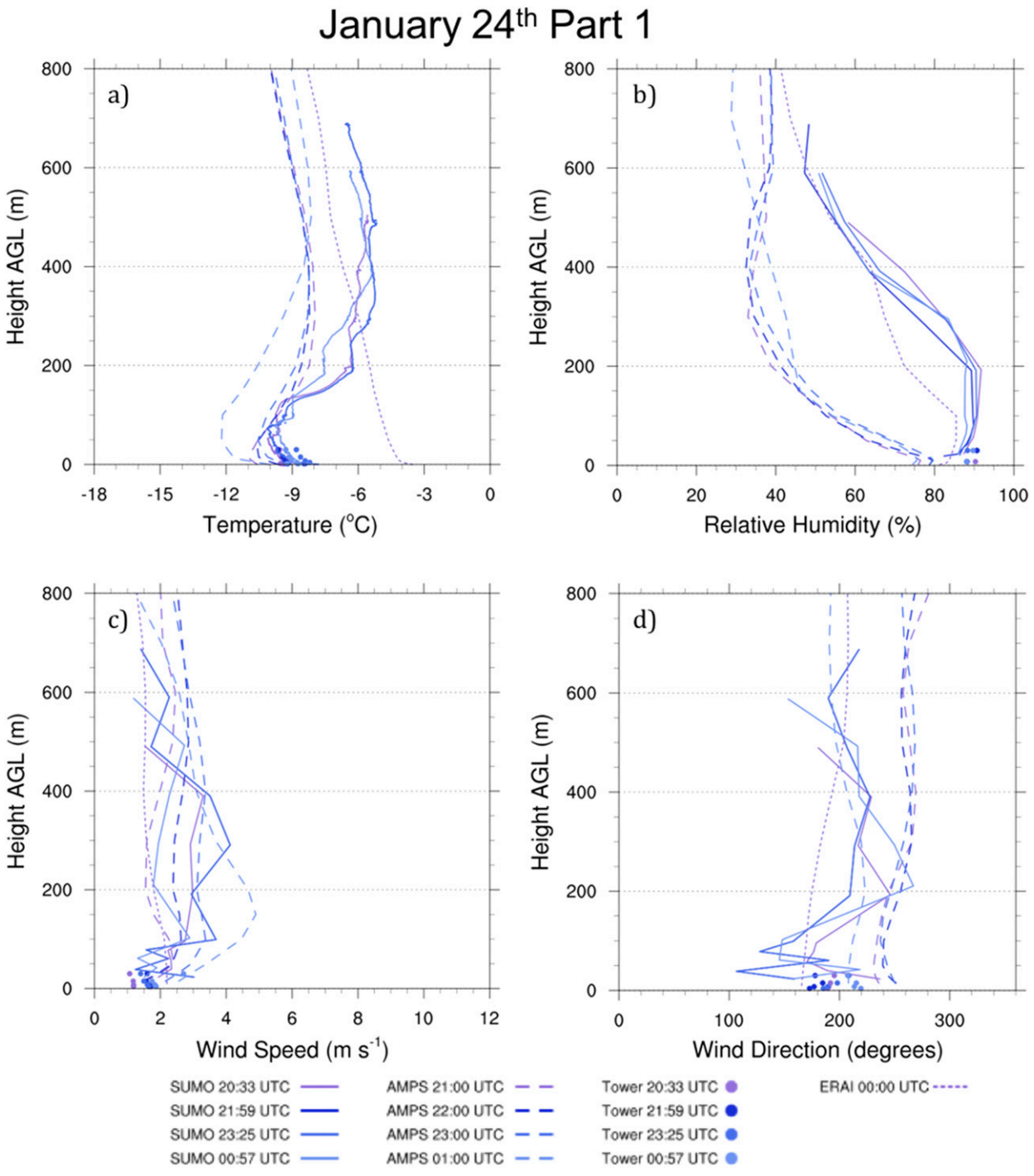

FIG. 12. As in Fig. 10, but for the 24 Jan first four SUMO flights.

underestimates the moisture content of the katabatic flow draining down the Transantarctic Mountains. As seen in Wille et al. (2016), katabatic flow from Byrd and Mulock Glacier to the southwest is the primary wind regime over the ATT site and responsible for the highest relative humidity biases. Either AMPS is overestimating the magnitude of the katabatic flow as seen in the high wind speed bias, underestimating the moisture content of the katabatic flow, or a combination of both. While the SUMO data indicate that AMPS had an average westward wind direction bias, it is difficult to quantify the impacts this has on the relative humidity bias since

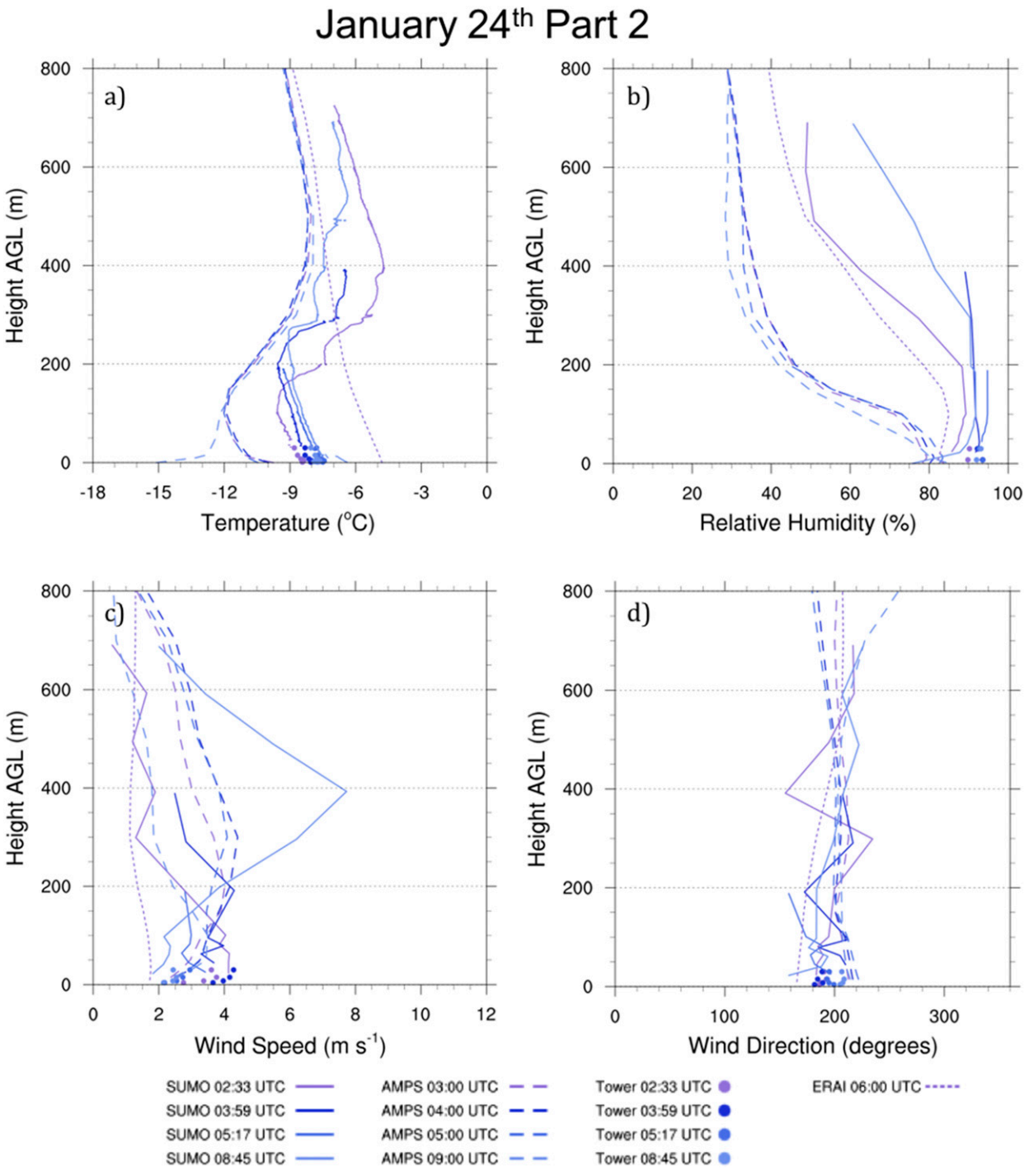

FIG. 13. As in Fig. 10, but for the 24 Jan last four SUMO flights.

Wille et al. (2016) noted a southward wind direction bias instead of the westward one observed in this study.

Since the dry biases appear to be related to the advection of unrealistically dry air from the Antarctic continent, it might explain why radiosonde studies at McMurdo found the AMPS moisture products to be generally accurate (Bromwich et al. 2005; Fogt and Bromwich 2008; Vázquez B. and Grejner-Brzezinska 2013) whereas another study found a dry bias over the Antarctic Plateau using the AMPS predecessor, polar-modified fifth-generation Pennsylvania State University–National Center for Atmospheric Research Mesoscale Model (Polar MM5),

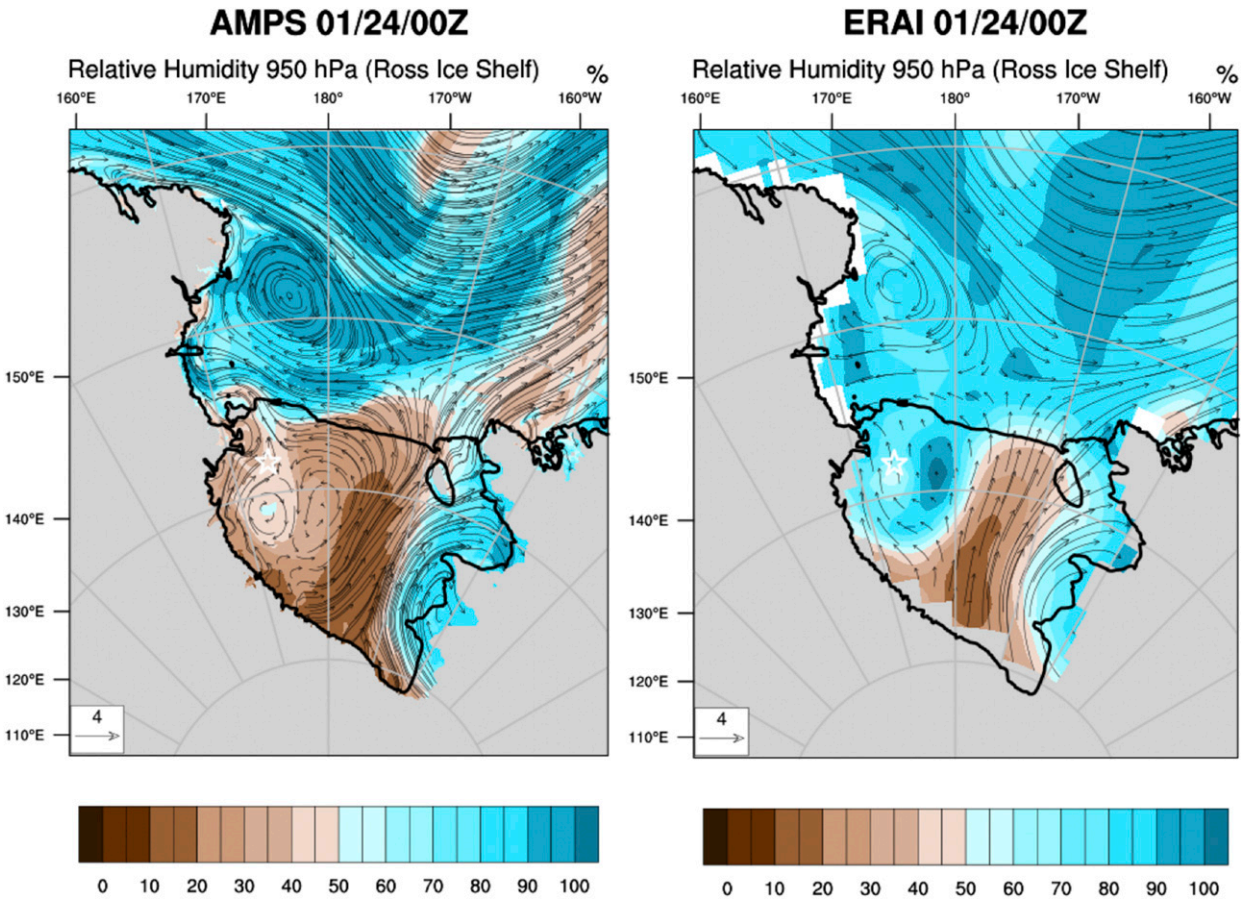

FIG. 14. As in Fig. 9, but for 0000 UTC 24 Jan.

which used the MYJ level-1.5 scheme (Guo et al. 2003). This is likely because of McMurdo's greater distance from the major katabatic drainage points along the Transantarctic Mountains like Byrd Glacier and its proximity to the Ross Sea. This suggests that the dry bias at the ATT site is related to the katabatic wind transporting an air mass from the Antarctic Plateau that has previously been determined to have a dry bias (Guo et al. 2003).

The three case studies discussed in this manuscript demonstrate the complexity of the circulation patterns over the Ross Ice Shelf, which makes it difficult to determine a simple cause for the errors seen in the AMPS simulations. However, the case studies in this study, including the ones not discussed in this manuscript, reveal a general high wind speed bias and a dry bias during katabatic flow events.

7. Conclusions

The results from this study and Wille et al. (2016) indicate the presence of a large dry bias in AMPS throughout the depth of the PBL. In the aforementioned study, the ATT–AMPS comparison revealed a modest near-surface dry bias regardless of seasonality. The SUMO flights showed the dry bias increases significantly past the height of the 30-m ATT. While this study focused on a couple weeks during the summer, it is likely this large moisture deficit extends year round, thus affecting the AMPS simulation of clouds on the Ross Ice Shelf. Wille et al. (2016) and this study also demonstrated that AMPS consistently overestimates the wind speed in the PBL. This wind speed bias, which reduces the stability of the PBL in the AMPS simulations, is likely related to the MYJ scheme as discussed in previous studies (Hines and Bromwich 2008; Tastula et al. 2012; Bromwich et al. 2013; Valkonen et al. 2014).

A significant dry bias in AMPS has major implications for Antarctic weather forecasters who rely on the AMPS relative humidity as a proxy for cloud forecasts over the ice and helps explain a source of problem with the AMPS cloud fraction products (Pon 2015). The highest relative humidity errors occur between 200 and 400 m,

which is around the same height that forecasters and aircraft operation managers carefully consider cloud cover for aircraft operations over the Antarctic continent. If the AMPS relative humidity product improved and in turn improved cloud forecasts over the ice, this could reduce the amount of costly aborted LC-130 missions over the Antarctic continent for USAP. In addition, accurately predicting the wind speed–stability relationship in AMPS is important for simulating vertical sensible and latent heat fluxes in the PBL, which influences cloud development. By misrepresenting the stability of the PBL, AMPS introduces errors in vertical motion and momentum fluxes, which has ramifications for aircraft encountering turbulence during takeoff and landing. Future Polar WRF PBL sensitivity studies should investigate the high wind speed bias and the resulting weakened PBL stability. To determine the source of the AMPS dry bias would require more PBL observations over the Antarctic Plateau. Despite the shortcomings in moisture and stability predictions, AMPS has generally high skill over Antarctica, especially in regards to resolving the katabatic flow, upper-atmospheric circulation, and temperature predictions.

Acknowledgments. We thank Linda Keller, David Mikolajczyk, Jonathan Thom, George Weidner, and Lee Welhouse from the University of Wisconsin–Madison for their help with the ATT AWS equipment, installation, maintenance, and the data. Our gratitude also extends to the USAP contractors who ensure field work like the SUMO UAS campaign are conducted in a safe and well-supported environment. The ATT and SUMO UAS campaign are supported by National Science Foundation (NSF) Grant ANT-1245663. The NSF via UCAR AMPS Grant GRT 0032749 to The Ohio State University and Grant ANT-1245737 to the University of Colorado Boulder funded this research.

REFERENCES

Antarctic Mesoscale Prediction System, 2015: Current AMPS configuration. UCAR, accessed 8 August 2016. [Available online at http://www2.mmm.ucar.edu/rt/amps/information/configuration/configuration.html.]

Bromwich, D. H., A. J. Monaghan, K. W. Manning, and J. G. Powers, 2005: Real-time forecasting for the Antarctic: An evaluation of the Antarctic Mesoscale Prediction System (AMPS). *Mon. Wea. Rev.*, **133**, 579–603, doi:10.1175/MWR-2881.1.

——, K. M. Hines, and L.-S. Bai, 2009: Development and testing of Polar Weather Research and Forecasting Model: 2. Arctic Ocean. *J. Geophys. Res.*, **114**, D08122, doi:10.1029/2008JD010300.

——, F. O. Otieno, K. M. Hines, K. W. Manning, and E. Shilo, 2013: Comprehensive evaluation of Polar Weather Research and Forecasting Model performance in the Antarctic. *J. Geophys. Res. Atmos.*, **118**, 274–292, doi:10.1029/2012JD018139.

Carrasco, J. F., and D. H. Bromwich, 1991: A case study of katabatic wind-forced mesoscale cyclogenesis near Byrd Glacier. *Antarct. J. U.S.*, **26** (5), 258–261.

——, and ——, 1994: Climatological aspects of mesoscale cyclogenesis over the Ross Sea and Ross Ice Shelf regions of Antarctica. *Mon. Wea. Rev.*, **122**, 2405–2425, doi:10.1175/1520-0493(1994)122<2405:CAOMCO>2.0.CO;2.

Cassano, J. J., 2014: Observations of atmospheric boundary layer temperature profiles with a small unmanned aerial vehicle. *Antarct. Sci.*, **26**, 205–213, doi:10.1017/S0954102013000539.

——, M. E. Higgins, and M. W. Seefeldt, 2011: Performance of the Weather Research and Forecasting (WRF) Model for month-long pan-Arctic simulations. *Mon. Wea. Rev.*, **139**, 3469–3488, doi:10.1175/MWR-D-10-05065.1.

Dee, D. P., and Coauthors, 2011: The ERA-Interim reanalysis: Configuration and performance of the data assimilation system. *Quart. J. Roy. Meteor. Soc.*, **137**, 553–597, doi:10.1002/qj.828.

Fogt, R. L., and D. H. Bromwich, 2008: Atmospheric moisture and cloud cover characteristics forecast by AMPS. *Wea. Forecasting*, **23**, 914–930, doi:10.1175/2008WAF2006100.1.

Guo, Z., D. H. Bromwich, and J. J. Cassano, 2003: Evaluation of Polar MM5 simulations of Antarctic atmospheric circulation. *Mon. Wea. Rev.*, **131**, 384–411, doi:10.1175/1520-0493(2003)131<0384:EOPMSO>2.0.CO;2.

Hines, K. M., and D. H. Bromwich, 2008: Development and testing of Polar Weather Research and Forecasting (WRF) Model. Part I: Greenland ice sheet meteorology. *Mon. Wea. Rev.*, **136**, 1971–1989, doi:10.1175/2007MWR2112.1.

——, and ——, 2017: Simulation of late summer Arctic clouds during ASCOS with Polar WRF. *Mon. Wea. Rev.*, **145**, 521–541, doi:10.1175/MWR-D-16-0079.1.

——, ——, L.-S. Bai, M. Barlage, and A. G. Slater, 2011: Development and testing of Polar WRF. Part III: Arctic land. *J. Climate*, **24**, 26–48, doi:10.1175/2010JCLI3460.1.

——, ——, L. Bai, C. M. Bitz, J. G. Powers, and K. W. Manning, 2015: Sea ice enhancements to Polar WRF. *Mon. Wea. Rev.*, **143**, 2363–2385, doi:10.1175/MWR-D-14-00344.1.

Jakobson, E., T. Vihma, T. Palo, L. Jakobson, H. Keernik, and J. Jaagus, 2012: Validation of atmospheric reanalyses over the central Arctic Ocean. *Geophys. Res. Lett.*, **39**, L10802, doi:10.1029/2012GL051591.

Janjić, Z. I., 1994: The step-mountain eta coordinate model: Further developments of the convection, viscous sublayer, and turbulence closure schemes. *Mon. Wea. Rev.*, **122**, 927–945, doi:10.1175/1520-0493(1994)122<0927:TSMECM>2.0.CO;2.

Jones, P. D., and D. H. Lister, 2015: Antarctic near-surface air temperatures compared with ERA-Interim values since 1979. *Int. J. Climatol.*, **35**, 1354–1366, doi:10.1002/joc.4061.

Lazzara, M. A., J. E. Thom, L. J. Welhouse, L. M. Keller, G. A. Weidner, M. Nigro, and J. J. Cassano, 2011: USAP Antarctic Automatic Weather Station Program status and field report. *Sixth Antarctic Meteorological Observation, Modeling, and Forecasting Workshop*. Hobart, Australia, Australian Bureau of Meteorology, 2 pp. [Available online at http://amrc.ssec.wisc.edu/abstracts/AMOMFW2011-Lazzara-AWS-final.pdf.]

——, G. A. Weidner, L. M. Keller, J. E. Thom, and J. J. Cassano, 2012: Antarctic Automatic Weather Station Program. *Bull. Amer. Meteor. Soc.*, **93**, 1519–1537, doi:10.1175/BAMS-D-11-00015.1.

Liu, Z., and D. H. Bromwich, 1997: Dynamics of the katabatic wind confluence zone near Siple Coast, West Antarctica. *J. Appl.*

Meteor., **36**, 97–118, doi:10.1175/1520-0450(1997)036<0097:DOTKWC>2.0.CO;2.

Mather, K. B., and G. S. Miller, 1967: Notes on topographic factors affecting the surface wind in Antarctica, with special reference to katabatic winds, and bibliography. University of Alaska Fairbanks Tech. Rep. UAG-R-189, 125 pp.

Mayer, S., G. Hattenberger, P. Brisset, M. Jonassen, and J. Reuder, 2012: A ''no-flow-sensor'' wind estimation algorithm for unmanned aerial systems. *Int. J. Micro Air Veh.*, **4**, 15–30, doi:10.1260/1756-8293.4.1.15.

Nigro, M. A., and J. J. Cassano, 2014: Identification of surface wind patterns over the Ross Ice Shelf, Antarctica, using self-organizing maps. *Mon. Wea. Rev.*, **142**, 2361–2378, doi:10.1175/MWR-D-13-00382.1.

——, ——, and S. L. Knuth, 2012a: Evaluation of Antarctic Mesoscale Prediction System (AMPS) cyclone forecasts using infrared satellite imagery. *Antarct. Sci.*, **24**, 183–192, doi:10.1017/S0954102011000745.

——, ——, M. A. Lazzara, and L. M. Keller, 2012b: Case study of a barrier wind corner jet off the coast of the Prince Olav Mountains, Antarctica. *Mon. Wea. Rev.*, **140**, 2044–2063, doi:10.1175/MWR-D-11-00261.1.

O'Connor, W. P., D. H. Bromwich, and J. F. Carraso, 1994: Cyclonically forced barrier winds along the Transantarctic Mountains near Ross Island. *Mon. Wea. Rev.*, **122**, 137–150, doi:10.1175/1520-0493(1994)122<0137:CFBWAT>2.0.CO;2.

Parish, T. R., and K. T. Waight III, 1987: The forcing of Antarctic katabatic winds. *Mon. Wea. Rev.*, **115**, 2214–2226, doi:10.1175/1520-0493(1987)115<2214:TFOAKW>2.0.CO;2.

——, and J. J. Cassano, 2003: The role of katabatic winds on the Antarctic surface wind regime. *Mon. Wea. Rev.*, **131**, 317–333, doi:10.1175/1520-0493(2003)131<0317:TROKWO>2.0.CO;2.

——, and D. H. Bromwich, 2007: Reexamination of the near-surface air flow over the Antarctic continent and implications on atmospheric circulations at high southern latitudes. *Mon. Wea. Rev.*, **135**, 1961–1973, doi:10.1175/MWR3374.1.

Pon, K., 2015: The representation of low cloud in the Antarctic Mesoscale Prediction System. M.S. thesis, Dept. of Geography, The Ohio State University, 80 pp.

Powers, J. G., 2009: Performance of the WRF V3.1 polar modifications in an Antarctic severe wind event. *10th WRF Users' Workshop*, Boulder, CO, NCAR, P3B.26. [Available online at www2.mmm.ucar.edu/wrf/users/workshops/WS2009/abstracts/P3B-26.pdf.]

——, K. W. Manning, D. H. Bromwich, J. J. Cassano, and A. M. Cayette, 2012: A decade of Antarctic science support through AMPS. *Bull. Amer. Meteor. Soc.*, **93**, 1699–1712, doi:10.1175/BAMS-D-11-00186.1.

Reddy, T. E., K. R. Arrigo, and D. M. Holland, 2007: The role of thermal and mechanical processes in the formation of the Ross Sea summer polynya. *J. Geophys. Res.*, **112**, C07027, doi:10.1029/2006JC003874.

Steinhoff, D. F., S. Chaudhuri, and D. H. Bromwich, 2009: A case study of a Ross Ice Shelf airstream event: A new perspective. *Mon. Wea. Rev.*, **137**, 4030–4046, doi:10.1175/2009MWR2880.1.

Tastula, E. M., T. Vihma, and E. L. Andreas, 2012: Evaluation of Polar WRF from modeling the atmospheric boundary layer over Antarctic sea ice in autumn and winter. *Mon. Wea. Rev.*, **140**, 3919–3935, doi:10.1175/MWR-D-12-00016.1.

Tewari, M., and Coauthors, 2004: Implementation and verification of the unified Noah land surface model in the WRF Model. *20th Conf. on Weather Analysis and Forecasting/16th Conf. on Numerical Weather Prediction*, Seattle, WA, Amer. Meteor. Soc., 11–15 pp.

Valkonen, T., T. Vihma, M. M. Johansson, and J. Launiainen, 2014: Atmosphere–sea ice interaction in early summer in the Antarctic: Evaluation and challenges of a regional atmospheric model. *Quart. J. Roy. Meteor. Soc.*, **140**, 1536–1551, doi:10.1002/qj.2237.

Vázquez B., G. E., and D. A. Grejner-Brzezinska, 2013: GPS-PWV estimation and validation with radiosonde data and numerical weather prediction model in Antarctica. *GPS Solutions*, **17**, 29–39, doi:10.1007/s10291-012-0258-8.

Wille, J. D., D. H. Bromwich, M. A. Nigro, J. J. Cassano, M. Mateling, M. A. Lazzara, and S.-H. Wang, 2016: Evaluation of the AMPS boundary layer simulations on the Ross Ice Shelf with tower observations. *J. Appl. Meteor. Climatol.*, **55**, 2349–2367, doi:10.1175/JAMC-D-16-0032.1.